THE JOURNAL OF BIOLOGICAL CHEMISTRY VOL. 286, NO. 26, pp. 22913–22923, July 1, 2011

Na^+ Channel *Scn1b* Gene Regulates Dorsal Root Ganglion Nociceptor Excitability *in Vivo*[*]

Received for publication, March 22, 2011, and in revised form, May 5, 2011 Published, JBC Papers in Press, May 9, 2011, DOI 10.1074/jbc.M111.242370

Luis F. Lopez-Santiago, William J. Brackenbury[1], Chunling Chen, and Lori L. Isom[2]

From the Department of Pharmacology, University of Michigan, Ann Arbor, Michigan 48109-0632

Nociceptive dorsal root ganglion (DRG) neurons express tetrodotoxin-sensitive (TTX-S) and -resistant (TTX-R) Na^+ current (I_{Na}) mediated by voltage-gated Na^+ channels (VGSCs). In nociceptive DRG neurons, VGSC β2 subunits, encoded by *Scn2b*, selectively regulate TTX-S α subunit mRNA and protein expression, ultimately resulting in changes in pain sensitivity. We hypothesized that VGSCs in nociceptive DRG neurons may also be regulated by β1 subunits, encoded by *Scn1b*. *Scn1b* null mice are models of Dravet Syndrome, a severe pediatric encephalopathy. Many physiological effects of *Scn1b* deletion on CNS neurons have been described. In contrast, little is known about the role of *Scn1b* in peripheral neurons *in vivo*. Here we demonstrate that *Scn1b* null DRG neurons exhibit a depolarizing shift in the voltage dependence of TTX-S I_{Na} inactivation, reduced persistent TTX-R I_{Na}, a prolonged rate of recovery of TTX-R I_{Na} from inactivation, and reduced cell surface expression of $Na_v1.9$ compared with their WT littermates. Investigation of action potential firing shows that *Scn1b* null DRG neurons are hyperexcitable compared with WT. Consistent with this, transient outward K^+ current (I_{to}) is significantly reduced in null DRG neurons. We conclude that *Scn1b* regulates the electrical excitability of nociceptive DRG neurons *in vivo* by modulating both I_{Na} and I_K.

VGSCs[3] comprise one pore-forming α subunit and two β subunits (β1–β4, encoded by *Scn1b–Scn4b*) that do not form the pore but play critical roles in channel subcellular localization, regulation of I_{Na}, VGSC gene transcription, and cell adhesive interactions leading to cytoskeletal modulation, changes in cell morphology, and cellular migration (1–3).

All four mammalian VGSC β subunit gene products are expressed in DRG neurons (4); however, little is known about their roles in nociception. The role of *Scn1b* in DRG neurons *in vivo* has not been investigated. *Scn1b* mRNA is expressed in DRG neurons (4), and the *Scn1b* splice variant β1B is expressed in adult rat DRG neurons as assessed by immunohistochemistry (5). *Scn1b* mRNA expression changes in the dorsal horn of the spinal cord in a model of neuropathic pain in rats (6), suggesting that β1/β1B are important in nociception. Despite this, the effects of β1 on the functioning of heterologously overexpressed sensory neuronal VGSCs are controversial. Initial reports of $Na_v1.7$ expression showed no functional effects of β1 (7, 8). Later, it was reported that co-expression of β1 with $Na_v1.7$ resulted in more rapid inactivation, hyperpolarizing shifts in the voltage dependence of activation and inactivation, and accelerated recovery from inactivation (9). Similarly, $Na_v1.8$ was originally reported to be unaffected by β1 (10). In the hands of another group, however, β1 plus $Na_v1.8$ co-expression resulted in more rapid inactivation, hyperpolarizing shifts in the voltage dependence of activation and inactivation, accelerated recovery from inactivation, and rapid entry into the slow inactivated state (9, 11). Heterologous expression of $Na_v1.9$ has been reported, but the effects of β subunits on this channel are not known (12).

Our goal here was to investigate the role of *Scn1b* in small DRG neurons *in vivo*. Taken together, our results suggest that *Scn1b* has complex effects on TTX-S and TTX-R I_{Na} as well as I_K in nociceptors and thus may be a reasonable target for future drug development. These data represent the first report of the physiological role of *Scn1b* in DRG neurons *in vivo*.

EXPERIMENTAL PROCEDURES

Preparation of DRG Neurons—The generation of *Scn1b* null mice was described previously (13). Animals used in the present study were bred from a congenic strain of $Scn1b^{+/-}$ mice that had been repeatedly backcrossed to C57BL/6 for at least 15 generations. Animals of both sexes were used. All animal experiments were performed in accordance with the guidelines of the University of Michigan Committee on Use and Care of Animals. L4/5 DRG neurons were acutely dissociated from P17–P19 WT or null littermate mice as reported previously (4). Dissociated neurons were incubated for 2–10 h prior to electrophysiological recording, with the first 2 h used to allow cells to settle and adhere to the bottom of the culture dishes or coverslips. The remaining 8-h recording period was sufficiently short to minimize changes in electrical properties that may occur in long term cultures.

Voltage Clamp Recording—Voltage clamp recordings were performed in the standard whole-cell configuration as described previously (4). Small DRG neurons were defined as

* This work was supported, in whole or in part, by National Institutes of Health Grants R01MH059980 (to L. L. I.) and 2P30DK34933 (from the University of Michigan Gastrointestinal Peptide Research Center to L. F. L.-S.). This work was also supported by a University of Michigan Center for Organogenesis Non-traditional Postdoctoral Fellowship (to W. J. B.).

[1] Present address: Dept. of Biology, University of York, Heslington, York, YO10 5DD, United Kingdom.

[2] To whom correspondence should be addressed: Dept. of Pharmacology, University of Michigan, 1301 MSRB III, 1150 W. Medical Center Dr., Ann Arbor, MI 48109-0632. Tel.: 734-936-3050; Fax: 734-763-4450; E-mail: lisom@umich.edu.

[3] The abbreviations used are: VGSC, voltage-gated Na^+ channel; I_{Na}, Na^+ current; I_K, K^+ current; I_{to}, transient outward current; G_{Na}, Na^+ conductance; DRG, dorsal root ganglion; TTX, tetrodotoxin; TTX-S, tetrodotoxin-sensitive; TTX-R, tetrodotoxin-resistant; AP, action potential; APD_{50}, action potential duration 50%; AHP, after hyperpolarization; pF, picofarads; C_m, cell capacitance; HP, holding potential; PB, phosphate buffer; P*n*, postnatal day *n*.

those with 12 pF < cell capacitance (C_m) < 42 pF. All cells were examined within 10–60 min after removal from the cell culture incubator.

Currents were low pass-filtered at 5 kHz with a four-pole Bessel filter and digitally sampled at 20 or 40 kHz. Capacitive transients were canceled with the amplifier circuitry, and linear leakage currents were digitally subtracted on-line with *P*/4 routines. Patch electrodes had resistances of 0.8–2.5 megaohms, and the series resistance was typically in the range of 1–5 megaohms. When appropriate, this was reduced by 40–60% using the compensation circuit of the amplifier. The holding potential (HP) was always −80 mV. Recordings were performed using pClamp 9 software (Axon Instruments).

To analyze the voltage dependence of channel activation, the Na^+ conductance (G_{Na}) was calculated. Peak current data for each cell were divided by the respective driving force ($V_m - V_{rev}$) and plotted against V_m and fit to a Boltzmann equation of the following form,

$$G_{Na} = G_{max}/(1 + \exp(-(V_m - V_{1/2})/k)) \quad \text{(Eq. 1)}$$

where G_{max} is the maximum G_{Na}, $V_{½}$ is the voltage at which 50% of the VGSCs are activated, and k is the slope of the curve. Steady-state inactivation was measured by applying a double pulse protocol, consisting of a 500-ms prepulse ranging from −120 to 20 mV (in 5 and 10 mV increments), followed by a test pulse to 0 mV. Each data set (a plot of peak I_{Na} during the 0 mV test pulse *versus* prepulse voltage) was fit with the summation of two Boltzmann equations of the following form,

$$I_{Na} = F_1/(1 + \exp((V_m - V^1_{1/2})/k_1)) + F_2/(1 + \exp((V_m - V^2_{1/2})/k_2)) \quad \text{(Eq. 2)}$$

where F_1 and F_2 are the fractions of the first and second components of inactivation, respectively. The most negative component (component 1) results from the TTX-S I_{Na}, whereas the other results from TTX-R I_{Na}. $V_{½}$ is the potential at which half of the I_{Na} was inactivated, and k is the slope factor for each component. The sum of both fractions is the calculated maximum I_{Na} ($F_1 + F_2 = I_{max}$). Data points were then normalized with respect to I_{max} to obtain the inactivation curve.

To examine the rate of channel recovery from inactivation, a protocol was designed comprising a 500-ms prepulse to −120 mV, followed by a test pulse to 0 mV, and then returning to −120 mV for a variable time period (0.25, 0.5, 1, 2, 4, 6, 8, 10, 20, 30, 40, 50, 75, 100, 200, 300, 400, 500, and 750 ms) before application of a second test pulse to 0 mV. The I_{Na} amplitude from the second 0-mV pulse was divided by the amplitude of the corresponding first test pulse to obtain the fraction of I_{Na} recovered after the recovery time. The data were fit with a double exponential equation of the following form,

$$I_{Na\,p2}/I_{Na\,p1} = f_1*(1 - \exp(-t/\tau_1)) + f_2*(1 - \exp(-t/\tau_2)) \quad \text{(Eq. 3)}$$

where $I_{Na\,p2}/I_{Na\,p1}$ is the fraction of current recovered; f_1 and f_2 are the fractions of fast and slow recovery components, respectively; t is recovery time; and τ_1 and τ_2 are the time constants for each recovery component.

AP Measurements—Isolated DRG neurons were bathed at RT in 1× HBSS (Invitrogen) supplemented with 20 mM HEPES, pH 7.3. Patch pipettes (1.0–3.0 megaohms) were filled with 135 mM KCl, 10 mM NaCl, 1 mM $CaCl_2$, 10 mM EGTA, and 10 mM HEPES, pH 7.4, with KOH. The resting potential (V_{rest}) was determined under current clamp at zero current. The stimulus to elicit an AP (threshold current) was determined by application of 3-ms test pulses every 2.5 s, starting at 0.1 nA and increasing by 0.1 nA until an AP was observed. Subsequent APs were evoked by application of 12 3-ms test pulses at 1.5× threshold (14). DRGs were paced at 1, 10, 6.6, 3.3, and finally 1 Hz, and for every cell the same sequence of protocols was used. Data from the threshold and 1 and 10 Hz protocols are reported. Current clamp recording was performed on *I-Clamp fast* mode on an Axopatch 200B amplifier (Molecular Devices). To quantify AP duration, the maximal spike amplitude was calculated as the voltage from overshoot to the after hyperpolarization (AHP) value followed by calculation of the absolute duration between depolarization and repolarization at 50% of the maximal spike amplitude (ADP_{50}) (Fig. 6*B*). Finally, the maximum rates of depolarization and repolarization were measured from the differentiated waveform.

Isolated K^+ Currents (I_K)—I_K were recorded from single, small DRG neurons at RT in the presence of a bath solution that contained 150 mM choline-Cl, 5 mM KCl, 1 mM $MgCl_2$, 0.1 mM $CdCl_2$, 10 mM HEPES, 10 mM glucose (pH 7.3 with KOH), and 1 μM TTX. Fire-polished patch pipettes were filled with an internal solution containing 100 mM KCl, 30 mM *N*-methyl-D-glucamine, 1 mM $CaCl_2$, 1 mM $MgCl_2$, 10 mM EGTA, 4 mM MgATP, 10 mM HEPES, and 10 mM glucose (pH 7.3 with HCl). To isolate I_{to}, a protocol with 150-ms test pulses ranging from −40 to 60 mV (in 10-mV increments) was applied twice, first with a prepulse to −110 and then with prepulse to −40 mV. Subtracting currents obtained using the −40 mV prepulse protocol from those obtained using the −110 mV prepulse protocol resulted in I_{to}.

Analysis of Electrophysiological Data—Data were analyzed using pClamp 9 (Axon Instruments) and Sigma Plot 10 or 11 (SPSS Inc., Chicago, IL). The statistical significance of differences between mean values for null and WT neurons was evaluated by Student's unpaired *t* test or χ^2, as indicated, with $p < 0.05$ considered significant. Results are presented as means ± S.E.

Immunohistochemistry—L4/5 DRGs from P14–P16 WT or null mice were fixed in 4% paraformaldehyde for 15 min, followed by cryoprotection in 10 and 30% sucrose, respectively, for 24 h. DRGs were then frozen in M1 embedding medium (Thermo Fisher Scientific, Waltham, MA). Sections were cut to a thickness of 20 μm on a Leica CM1850 cryostat, mounted on glass slides, and stored at −20 °C until use. Tissue sections were washed three times in 0.1 M phosphate buffer (PB), followed by blocking for 1 h in PBTGS (10% normal goat serum and 0.3% Triton X-100 in 0.1 M PB). Sections were incubated overnight with primary antibodies diluted in PBTGS: polyclonal rabbit anti-$Na_v1.8$ (1:200; Alomone, Jerusalem, Israel), polyclonal rabbit anti-$Na_v1.9$ (1:400; a gift from Dr. Patrick Delmas, Laboratoire de Neurophysiologie Cellulaire, Faculté de Médecine IFR Jean Roche, Marseille, France), or monoclonal mouse anti-

peripherin (1:200; Millipore, Temecula, CA). After three washes in 0.1 M PB, sections were incubated for 2 h with Alexafluor 488 anti-mouse and Alexafluor 594 anti-rabbit antibody (1:500 in PBTGS; Invitrogen). Sections were then washed once in 0.1 M PB and then incubated for 5 min in 4′,6-diamidino-2-phenylindole (DAPI; 10 μg/ml; Sigma), followed by two additional washes in 0.1 M PB. The sections were dried and mounted (Gel/Mount; Biomeda, Foster City, CA).

Confocal Microscopy and Image Analysis—Samples were viewed using an Olympus Fluoview 500 confocal laser scanning microscope with 100× objectives in the University of Michigan Department of Pharmacology. Images (512 × 512 pixels) were initially processed with the Olympus Optical Fluoview software and then exported into ImageJ (National Institutes of Health, Bethesda, MD) and/or Adobe Photoshop. Ten images each of DRG sections colabeled with anti-$Na_v1.8$ or anti-$Na_v1.9$ and anti-peripherin were analyzed per mouse, for a total of three WT and three null mice. The percentage of small DRG neurons expressing $Na_v1.8$ or $Na_v1.9$ was calculated from those images. In addition, for each image, the number of peripherin-positive neurons that also expressed $Na_v1.8$ or $Na_v1.9$ was counted and expressed as a percentage. Data were combined to provide an overall mean and S.E.

The subcellular distribution of $Na_v1.8$ and $Na_v1.9$ labeling in small neurons was analyzed using a method similar to those described previously (15–17). Briefly, for each image and using ImageJ software, two straight lines were drawn across well defined cells, avoiding the nucleus. A profile of signal intensity was obtained for each line, and then using Clampfit 9.2 software (Axon Instruments), the signal intensity was calculated as the area under the curve. Signal intensity in the plasma membrane region, defined as 0.75 μm inward from the outer edge of labeling, was compared with average cytoplasmic signal intensity of equivalent internal length.

RESULTS

Identification and Definition of Neuronal Size—We measured C_m of 20.0 ± 1.6 pF ($n = 34$) for WT and 16.28 ± 0.9 pF ($n = 29$) for null neurons ($p = 0.051$) (4, 18, 19). On average, *Scn1b* null neurons exhibited a slightly smaller C_m than WT neurons. This difference may reflect the overall small size of *Scn1b* null mice compared with their WT littermates (13).

Using a well established voltage clamp protocol based on previously observed differences in voltage gating properties between TTX-S and TTX-R VGSCs expressed in DRG neurons (4, 20), two types of I_{Na} were dissected from the total I_{Na}. Briefly, a current-voltage (*I*-V) protocol with a 500-ms prepulse to −120 or −50 mV followed by a test pulse from −100 to +40 mV was applied, with steps of 5 and 10 mV, waiting 10 s between each step (Fig. 1*A*, *inset*). Following application of a −120 mV prepulse, total I_{Na}, the sum of TTX-S and TTX-R I_{Na}, was recorded (Fig. 1*A*, *upper traces*). A second *I*-V protocol was then applied to the same cell but with a −50 mV prepulse to inactivate TTX-S I_{Na}, resulting in the TTX-R component of I_{Na} (Fig. 1*A*, *middle traces*). TTX-S I_{Na} was subsequently calculated by digital subtraction (Fig. 1*A*, *lower traces*). The holding potential was −80 mV for all of the recordings. This experiment classified small DRG neurons into two subgroups: "small fast" and "small slow," as described previously for *Scn2b* null neurons (4). If the maximum amplitude of TTX-S I_{Na} was greater than 70% of the total I_{Na} for a given cell, that cell was placed in the small fast subgroup (4, 18). These cells made up 65% (13 of 20) of the WT small cell population and 44% (10 of 23) of the *Scn1b* null small neurons. Cells placed in the small slow subgroup had TTX-R I_{Na} greater than 70% of the total I_{Na}. These cells made up 30% (6 of 20) of the WT and 48% (11 of 23) of the *Scn1b* null small cells. Cells that did not clearly fall into either category (5–8%) were not included in our analysis. The proportions of small fast and small slow cells between genotypes were not statistically significant (χ^2, $p = 0.1838$).

Effect of Scn1b Deletion on I_{Na} Voltage-dependent Properties—I_{Na} densities for both genotypes as a function of command voltage are plotted in Fig. 1*B* for small fast neurons and in Fig. 1*C* for small slow neurons. We did not observe significant changes in the density of TTX-S (*squares*) or TTX-R (*circles*) I_{Na} for either small fast (Fig. 1*B*; $n = 13$ for WT, *black*, *solid symbols*; $n = 10$ for *Scn1b* null, *gray*, *open symbols*) or small slow DRG neurons (Fig. 1*C*; $n = 6$ for WT, *black*, *solid symbols*; $n = 11$ for *Scn1b* null, *gray*, *open symbols*). There were no differences in the total I_{Na} (TTX-S plus TTX-R) for small fast (Inset Fig. 1*B*) or small slow neurons (data not shown) between genotypes. Further, we observed no differences in the current-voltage curves between *Scn1b* null and WT neurons when small DRG neurons were pooled, regardless of fast or slow classification. These results suggested that there were no compensatory changes in the expression of VGSCs responsible for transient I_{Na} resulting from *Scn1b* deletion. Based on these data, all subsequent electrophysiological results in this study are reported for the pooled group (slow plus fast) of small neurons. Analyses of each subgroup were performed with similar conclusions but are not shown.

To analyze the voltage dependence of channel activation, the Na^+ conductance (G_{Na}) was calculated as described under "Experimental Procedures." For WT (*solid symbols*, $n = 19$) and *Scn1b* null (*open symbols*, $n = 21$) small DRG neurons (Fig. 2, *A* and *C*), all mean values for current activation, G_{max}, $V_{½}$ (Fig. 2*C*), and k were similar for both TTX-R (*gray*) and TTX-S (*black*) I_{Na} between groups. These results again suggested that *Scn1b* does not regulate cell surface levels of VGSCs that contribute to transient I_{Na} in DRG neurons.

Steady-state inactivation was measured as described under "Experimental Procedures." An example of I_{Na} obtained from a typical small WT neuron in response to a test pulse to 0 mV is shown in the *inset* to Fig. 2*B*. In this example, as in practically all small DRG neurons tested and in previous reports (4, 18, 20), the fast I_{Na} (TTX-S) inactivated at more negative voltages than the slow I_{Na} (TTX-R). Inactivation curves shown were generated from the same cells used to calculate activation curves in Fig. 2*A*. The corresponding $V_{½}$ values are compared in Fig. 2*D*. The $V_{½}$ of inactivation for TTX-R I_{Na} (in small *Scn1b* null neurons (*open symbol*) was not significantly different from that measured in small WT neurons (*solid symbol*) ($p = 0.088$; Fig. 2*D*). In contrast, $V_{½}$ for TTX-S I_{Na} in the *Scn1b* null neurons was shifted 10.8 mV in the depolarizing direction ($p = 0.048$; Fig. 2, *B* and *D*) compared with WT. Similar results were obtained using an alternative analysis in which independent

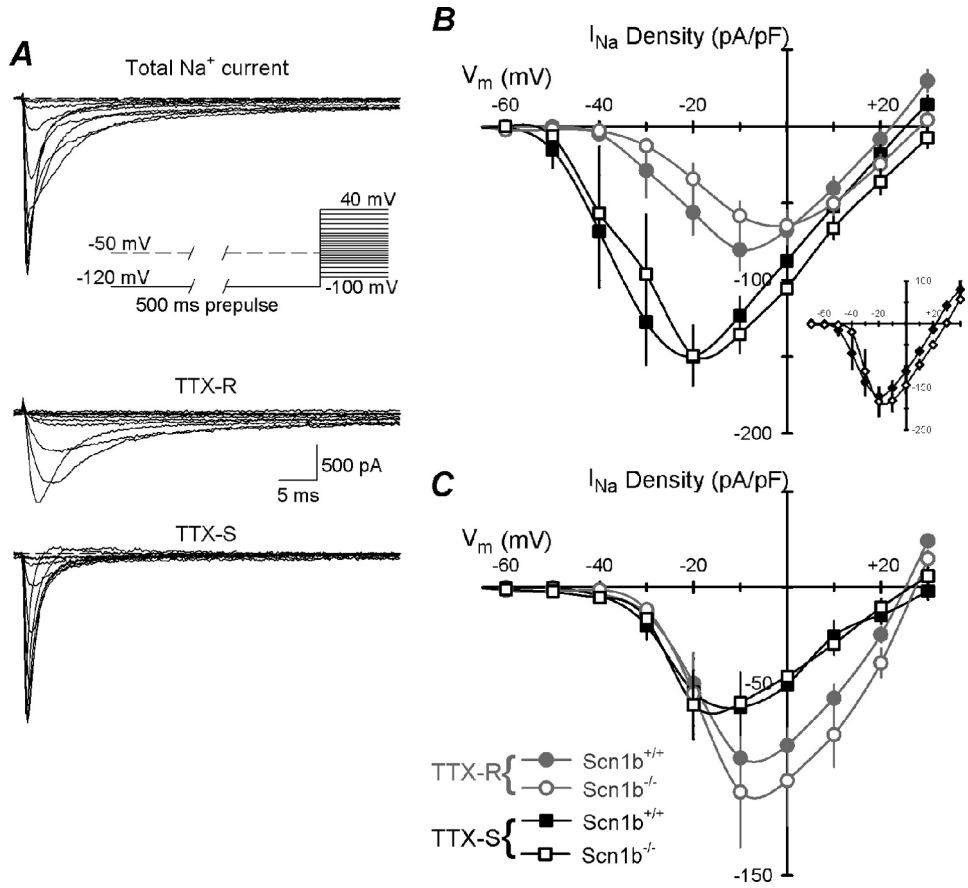

FIGURE 1. **Current-voltage relationships.** *A*, protocol for separation of TTX-R and TTX-S I_{Na} values. A 500-ms prepulse to −120 or −50 mV was applied before a 50-ms test pulse from −100 to 40 mV with steps of 5 or 10 mV (*inset*). Currents evoked from a typical WT small fast DRG neuron by test pulses from −50 to 0 mV are shown. Both TTX-S and TTX-R I_{Na} values were apparent after the −120 mV prepulse (*upper traces*). Only TTX-R I_{Na} values were obtained following the −50 mV prepulse (*middle traces*). The TTX-S component was obtained (*lower traces*) by digitally subtracting the TTX-R I_{Na} from the total I_{Na} *B*, average peak I_{Na} density-voltage relationships for TTX-R I_{Na} values (*circles*) and TTX-S I_{Na} values (*squares*) of small fast DRG neurons, WT (*closed symbols*, $n = 13$) or *Scn1b* null (*open symbols*, $n = 10$). *Inset*, *I*-V curves of total I_{Na} from the same cells as in *B*: WT (*closed symbols*) and *Scn1b* null (*open symbols*). *C*, similar to *B* but for small slow neurons, WT (*closed symbols*, $n = 6$) or *Scn1b* null (*open symbols*, $n = 11$). For this and all figures, data are presented as mean ± S.E. (*error bars*).

inactivation curves for TTX-S and TTX-R I_{Na} were calculated (not shown) (4).

The rate of channel recovery from inactivation was measured as described under "Experimental Procedures" (Fig. 2*E*). In agreement with previous reports, the time course of recovery from inactivation exhibited two components, with TTX-R I_{Na} recovering faster than TTX-S I_{Na} (20, 21). The time constants for recovery were as follows: WT $\tau_{fast} = 0.80 \pm 0.09$ ms and $\tau_{slow} = 105.03 \pm 19.96$ ms; *Scn1b* null $\tau_{fast} = 1.47 \pm 0.30$ ms and $\tau_{slow} = 56.55 \pm 12.26$ ms. τ_{fast} was significantly prolonged for *Scn1b* null compared with WT neurons ($p = 0.043$), suggesting a change in the kinetics of TTX-R I_{Na} in response to the null mutation. In contrast, τ_{slow} as well as the fractions of each component present in each genotype were not significantly different ($p > 0.05$).

Persistent I_{Na} Is Altered in Scn1b Null Neurons—DRG neurons express both transient and persistent I_{Na}, with the TTX-R channels $Na_v1.8$ and $Na_v1.9$ contributing significantly to these two components, respectively (22, 23). To examine changes in persistent I_{Na} in response to *Scn1b* deletion, we first applied a 50 ms long depolarizing pulse to 0 mV to record both transient and persistent I_{Na} (Fig. 3*A*). We observed no changes in the density of I_{Na} in *Scn1b* null neurons compared with WT at the peak of the transient I_{Na} ($p = 0.413$; Fig. 3*B*). In contrast, the persistent I_{Na}, measured as the average density of current during the last 2 ms of the test pulse, was reduced ~40% in *Scn1b* null neurons compared with WT ($p = 0.025$; Fig. 3*B*). We confirmed this difference by analyzing the density of the tail current, measuring VGSCs that were available to conduct at the end of the test pulse (Fig. 3*A*). The density of the tail I_{Na} was smaller in *Scn1b* null neurons (−121.3 ± 14.6 pA/pF, $n = 21$) compared with WT (−176.4 ± 17.0 pA/pF, $n = 19$), and this difference was statistically significant ($p = 0.018$; Fig. 3*B*).

To evaluate the kinetics of current inactivation, the decaying phase of I_{Na} was fit with a double exponential function, obtaining two inactivation time constants, τ_{fast} and τ_{slow}. We observed no significant changes in the values of either of these constants between genotypes ($p = 0.334$ and $p = 0.123$; Fig. 3*C*). Further, there were no changes in the proportion of the fast or slow components between genotypes (not shown). To quantify the rate of deactivation, the decaying phase of the tail I_{Na} was fit with a double exponential function (Fig. 3*D*). Although there were no changes in τ_{slow} for deactivation, we observed that τ_{fast} for deactivation was significantly smaller for *Scn1b* null neurons compared with WT ($p = 0.015$). The proportions of slow and fast deactivating current were unchanged between geno-

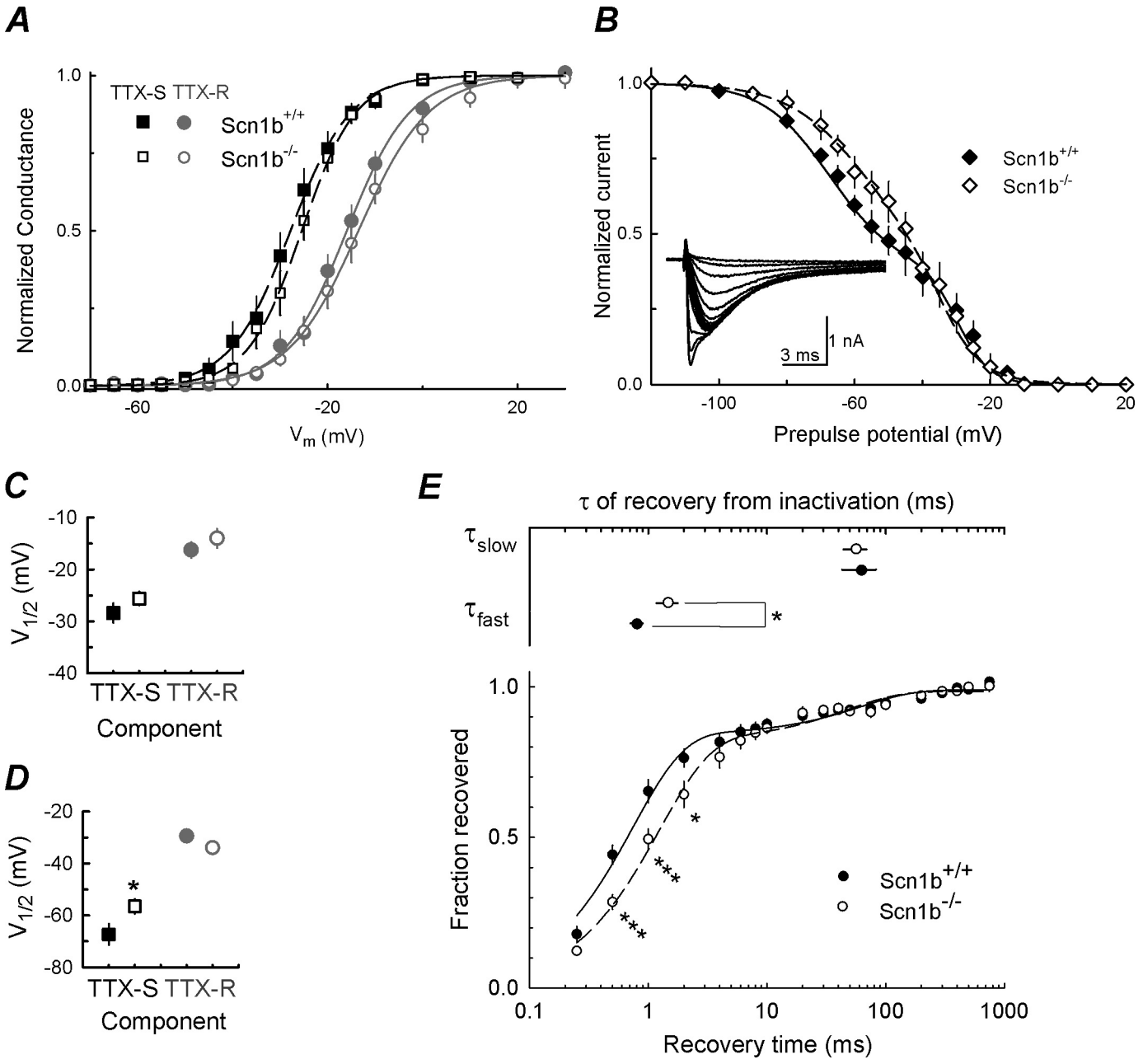

FIGURE 2. **Voltage dependence of activation and inactivation curves and recovery from inactivation.** *A*, activation curve of peak Na^+ conductance: TTX-R (*circles*) and TTX-S (*squares*) obtained from the same neurons as in Fig. 1, WT (*closed symbols*; $n = 19$), and *Scn1b* null (*open symbols*; $n = 21$). *Smooth lines* are fits to a Boltzmann function for TTX-R (*dashed lines*) and TTX-S (*solid lines*) currents, respectively. *B*, steady-state inactivation curves: peak I_{Na} at 0 mV, normalized to its maximal value (*inset*), as a function of voltage during the 500-ms prepulse. I_{Na} values were measured from the same WT (*closed symbols*) and *Scn1b* null (*open symbols*) small DRG neurons as in *A*. Each data set was fit with a double Boltzmann function (*lines*). *Inset*, example of I_{Na} at 0 mV, from one small WT cell, after 500-ms prepulses from −90 to −10 mV. *C*, midpoint potential ($V_{1/2}$) of fitted activation curves. *D*, $V_{1/2}$ of fitted inactivation curves shown in *B*; *squares* represent the first component (TTX-S), and *circles* represent the second component (TTX-R). *, values significantly different from WT, $p < 0.05$. *E*, *Scn1b* null small DRG neurons exhibit delayed recovery from inactivation. *Top*, τ_{slow} and τ_{fast} for recovery from inactivation for WT (*closed symbols*) and *Scn1b* null (*open symbols*) neurons. *Bottom*, average time course of recovery from inactivation for total I_{Na} for WT (*closed symbols*; $n = 13$) and *Scn1b* null (*open symbols*; $n = 13$) neurons. The protocol used included two test pulses to 0 mV with prepulse and interpulse V_m values of −120 mV and recovery intervals from 0.25 to 750 ms. Data were fitted with a double exponential (*lines*). Significant differences from WT are indicated as follows: *, $p < 0.05$; ***, $p < 0.001$.

types (not shown). These results suggested that *Scn1b* deletion may affect the expression or subcellular localization of the VGSC known to be responsible for persistent or slow inactivating I_{Na} in DRG neurons, $Na_v1.9$ (24).

Scn1b Modulates Slow Inactivating I_{Na}—To analyze the role of *Scn1b* in regulation of persistent or slow inactivating I_{Na} in greater detail, we used 2-s ramp protocols from −100 to 50 mV with a change of 0.075 mV/ms (Fig. 4*A*, *top trace*) to record instantaneous *I*-V curves of very slow inactivating and persistent currents (Fig. 4*A*). Using this method, we observed a 42% reduction in the maximum amplitude of this current in *Scn1b* null neurons compared with WT, with no change in voltage dependence. In a second series of experiments, we used a double pulse protocol consisting of a pulse to 0 mV followed by a

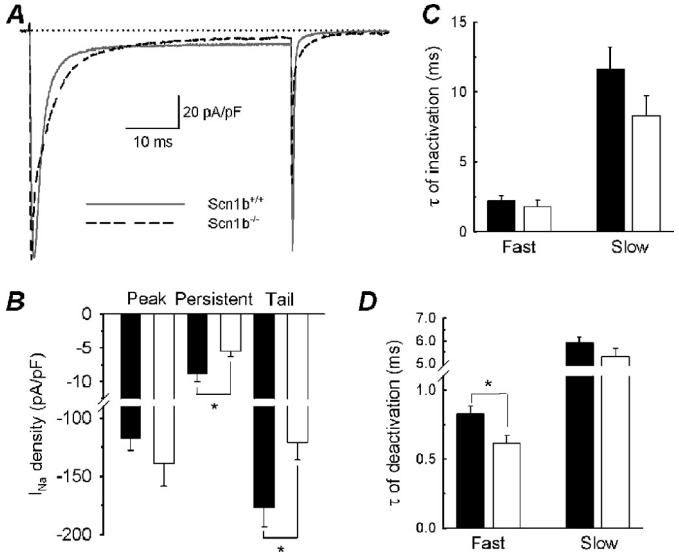

FIGURE 3. **I_{Na} density and kinetics at 0 mV.** *A*, representative I_{Na} values evoked by a test pulse to 0 mV from a holding potential of −80 mV. *Solid gray line*, WT; *dashed black line*, *Scn1b* null. *B*, peak, persistent, and tail I_{Na} density. Peak is defined as the maximum I_{Na} after applying a test pulse to 0 mV. Persistent I_{Na} is the average current density measured from 48 to 50 ms following the test pulse. Tail I_{Na} is the current measured at the end of the test pulse in response to repolarization to −80 mV. The data were obtained from the same neurons used in Figs. 1 and 2. *Black bars*, WT; *white bars*, *Scn1b* null. *C*, time constants of I_{Na} inactivation. The two time constants of inactivation (τ_{fast} and τ_{slow}) were obtained by fitting the decay phase of the I_{Na} with a double exponential function. *Black bars*, WT; *white bars*, *Scn1b* null; not significant differences. *D*, time constants of I_{Na} deactivation. Similar to *C*, the two time constants were obtained by fitting the decay phase of the tail I_{Na} with a double exponential function. *Black bars*, WT; *white bars*, *Scn1b* null; *, a significant difference from WT, $p < 0.05$. *Error bars*, S.E.

conditioning pulse of variable duration (10 ms to 16 s) and a test pulse of 25-ms duration (Fig. 4*B*, *inset*). The current generated from the second pulse (not inactivated) was normalized to the first pulse (total current). Data were fit with a double exponential equation, resulting in two constants for inactivation: one on the order of 100 ms for slow inactivation and another on the order of 1.5 s for ultraslow inactivation (Fig. 4*B*). Slowly inactivating I_{Na} was observed to constitute the largest fraction of the total I_{Na} measured using this method for both genotypes (Table 1). Further, this current was modulated by *Scn1b* expression (36% increase, $p = 0.039$). In contrast, the ultraslow and persistent I_{Na} values recorded using this double pulse protocol were not significantly changed in the absence of *Scn1b* ($p = 0.118$ and 0.516, respectively; Table 1 and Fig. 4*B*).

$Na_v1.9$ Expression and Subcellular Localization Are Altered in Scn1b Null Neurons—Our electrophysiological measurements predicted that *Scn1b* deletion may result in a change in expression or subcellular localization of $Na_v1.9$. Using specific antibodies recognizing $Na_v1.8$, $Na_v1.9$, or peripherin, immunohistochemistry was performed on 20-μm L4/5 DRG sections isolated from *Scn1b* null or WT mice (Fig. 5). Double labeling with anti-peripherin was used to analyze the populations of neurons expressing these two TTX-R channels in small DRG neurons (25). As reported previously (26), we observed that $Na_v1.8$ (Fig. 5*A*, *red*) and $Na_v1.9$ (Fig. 5*B*, *red*) are expressed in both large and small DRG neurons, with anti-peripherin (Fig. 5, *A* and *B*, *green*) identifying the small neurons. DAPI staining (*blue*) was used to identify cell nuclei. The percentages of

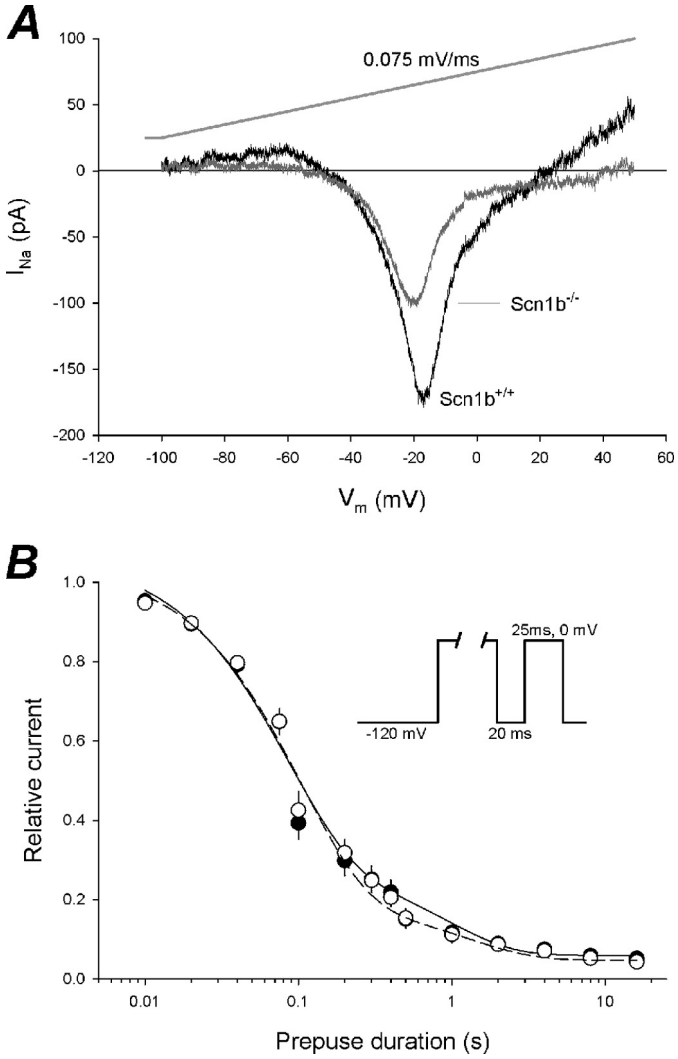

FIGURE 4. **Persistent and slowly inactivating I_{Na}.** *A*, average instantaneous *I*-V curves of slowly inactivating I_{Na} from WT ($n = 5$) and *Scn1b* null ($n = 6$) neurons. I_{Na} was recorded using a 2-s voltage ramp (*gray line*). *B*, I_{Na} availability as a function of prepulse duration in WT (*black circles*; $n = 12$) and *Scn1b* null (*open circles*; $n = 9$) neurons. Slow inactivation was induced by holding the cells at 0 mV for increasing durations of prepulse followed by a test pulse after brief repolarization. Data were fitted with a double exponential equation. *Solid line*, WT; *dashed line*, *Scn1b* null.

TABLE 1

Slow inactivation parameters from the double exponential fit of I_{Na} availability

Parameter	WT	*Scn1b* null	*p* value
f_f	0.771 ± 0.080	0.849 ± 0.023	0.428
τ_s (s)	0.085 ± 0.005	0.116 ± 0.015	0.039
f_s	0.238 ± 0.079	0.149 ± 0.014	0.300
τ_{us} (s)	1.255 ± 0.153	1.983 ± 0.475	0.118
I_p	0.060 ± 0.013	0.048 ± 0.011	0.516

peripherin-positive $Na_v1.8$-labeled cells and peripherin-positive $Na_v1.9$-labeled cells were similar for WT and *Scn1b* null sections, calculated for 30 DRG images from three mice of each genotype (Fig. 5*C*), suggesting that these neuronal populations were not altered by the *Scn1b* null mutation.

We next quantified the intensity of anti-$Na_v1.8$ or anti-$Na_v1.9$ labeling in small, peripherin-positive neurons using a technique previously reported to calculate a densitometry profile of VGSCs across the cell (Fig. 6*A*, *inset*) (15–17). We defined

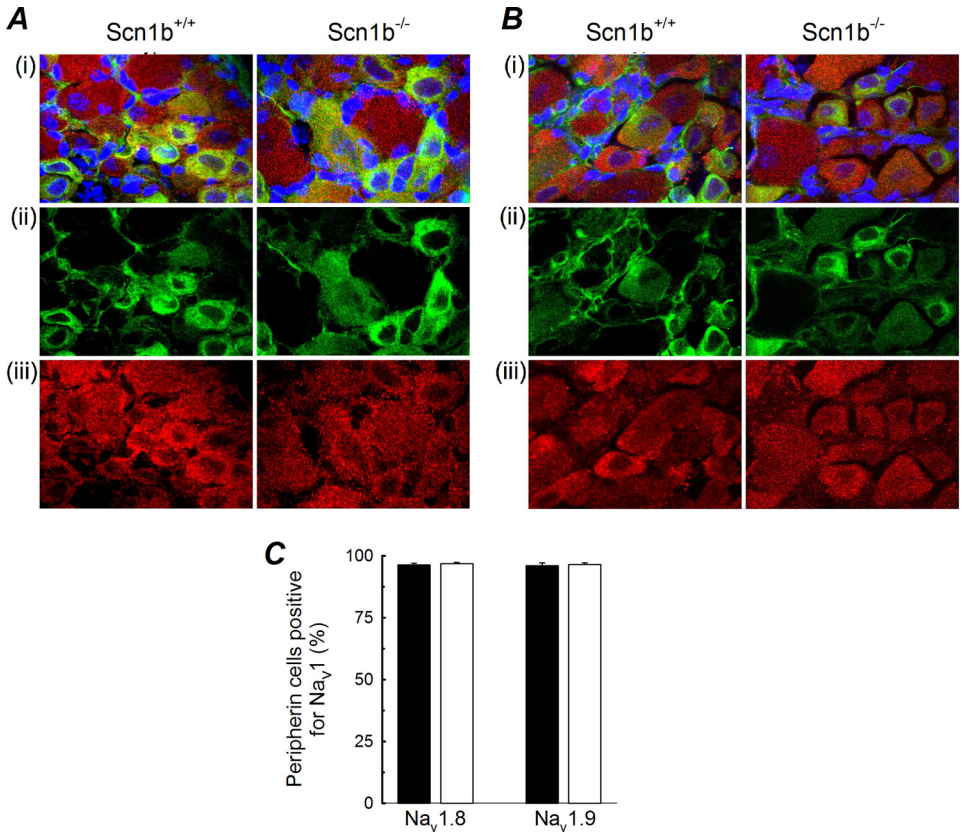

FIGURE 5. **TTX-R VGSC expression in small DRG neurons.** *A*, confocal images (×100) of 20-μm DRG sections from WT (*left*) or *Scn1b* null (*right*) mice, stained with anti-$Na_v1.8$ (*red*, *iii*) or peripherin (*green*, *ii*). The merged image (*i*) includes nuclear staining by DAPI (*blue*). *B*, similar to *A*, except *row iii* demonstrates anti-$Na_v1.9$ labeling. *C*, percentage of cells positive for peripherin and $Na_v1.8$ or $Na_v1.9$, as indicated, for WT (*black*) or *Scn1b* null (*white*) DRGs. 30 images from three mice of each genotype for each VGSC α subunit antibody were analyzed.

the area within 0.75 μm of the cell surface as the plasma membrane region. The results of this measurement for a typical WT cell are shown in Fig. 6*A*. The areas in *gray*, delimited by the *red lines* on *either side* of the plot, are defined as the plasma membrane regions. Using this method, we observed a reduction in the localization of $Na_v1.9$ to the defined plasma membrane region in peripherin-positive *Scn1b* null DRG neurons compared with WT ($p = 0.00002$). Fig. 6*B* shows the results of a single experiment ($n = 8$ cells/genotype), in which we observed a significant reduction in anti-$Na_v1.9$ signal intensity ($p = 0.0054$) in the defined plasma membrane region for *Scn1b* null neurons compared with WT. Further, we observed a significant reduction in anti-$Na_v1.9$ signal intensity inside the cell (area to the *right* of the *red line* in Fig. 6*B*) ($p = 0.047$). The data reached greater significance when the results of three independent experiments were averaged (Fig. 6*C*, $n = 24$ cells/genotype), in which we observed a 30% reduction in $Na_v1.9$ plasma membrane signal intensity in the null neurons compared with WT ($p = 5.27 \times 10^{-6}$) as well as a 25% reduction in $Na_v1.9$ signal intensity in the defined intracellular region ($p = 2.27 \times 10^{-6}$). Similar analysis of anti-$Na_v1.8$ labeling in peripherin-positive neurons (Fig. 6*D*) revealed no significant changes in the localization of this channel to the defined plasma membrane region ($p = 0.55$), although we did observe a reduction in the defined intracellular anti-$Na_v1.8$ signal intensity in the null neurons compared with WT ($p = 0.006$). These results suggested that the overall expression levels of $Na_v1.8$ and $Na_v1.9$ protein are reduced in *Scn1b* null neurons. However, of these two channels, only the cell surface expression of $Na_v1.9$ appears to be affected by the null mutation, consistent with the observed functional reduction in persistent I_{Na}.

Excitability of Small DRG Neurons Is Altered in Scn1b Null Mice—To assess the contribution of *Scn1b* to resting membrane potential and AP properties, we performed current clamp recordings from acutely dissociated small DRG neurons of both genotypes. APs were induced by injecting depolarizing current pulses into the cell. We observed large APs with characteristic shoulders, as described previously for nociceptors (27). The current necessary to evoke a single AP (threshold current) was similar for WT (0.282 ± 0.018 nA, $n = 11$) and *Scn1b* null (0.250 ± 0.029 nA, $n = 12$) neurons; however, the shape of the resulting APs was altered between genotypes (Fig. 7*A*). The values for the resting potential (V_{rest}), overshoot amplitude, and AHP were similar for neurons of both genotypes (Fig. 7*B*). However, the absolute difference between V_{rest} and AHP was significantly smaller for null neurons (20.8 ± 2.1 mV for WT *versus* 14.7 ± 1.7 mV for *Scn1b* null, $p = 0.038$), suggesting that null neurons become less hyperpolarized at the end of the AP than WT and are thus more available to fire subsequent APs. Further, the AP duration measured at the midpoint of the maximal spike amplitude (ADP_{50}) was significantly reduced in the null neurons (5.96 ± 0.44 ms for WT and 4.39 ± 0.38 ms for null, $p = 0.014$), again suggesting greater availability for subsequent AP firing. To analyze these changes in greater

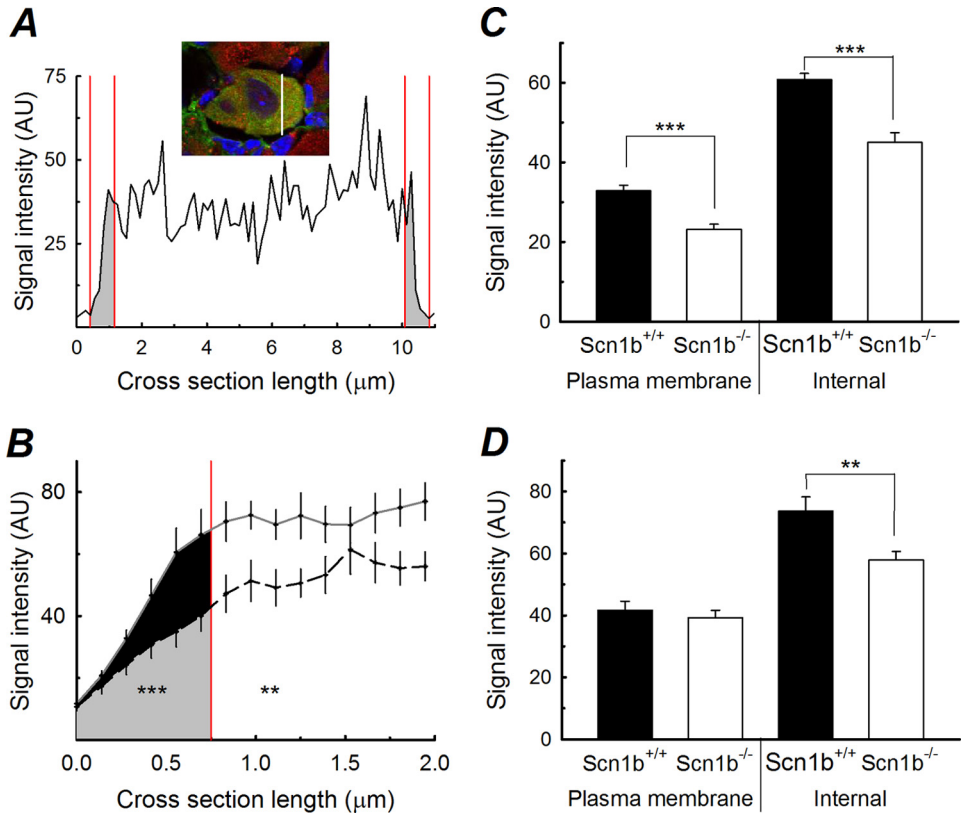

FIGURE 6. **Surface expression of $Na_v1.9$ is reduced in *Scn1b* null small DRG neurons.** *A*, typical densitometry profile in arbitrary units (*AU*) calculated along the *white line* drawn across the WT cell shown in the *inset*. In the plot, the areas in *gray* are defined as the plasma membrane region (0.75 μm from each edge of the cell). *Inset*, WT neuron inmunopositive for peripherin (*green*) and $Na_v1.9$ (*red*). Nuclear staining by DAPI (*blue*). *B*, average profile of $Na_v1.9$ expression for one experimental group of cells. Plasma membrane area is shown in *black* for WT and in *gray* for *Scn1b* null ($n = 32$ edges for eight cells of each genotype). *C*, summary of anti-$Na_v1.9$ staining in peripherin-positive cells calculated as in *A* and *B* for three experiments. *Black bars*, WT; *white bars*, *Scn1b* null ($n = 24$ cells/genotype). *D*, summary of anti-$Na_v1.8$ staining in peripherin-positive cells, calculated as in *A* and *B* for three experiments. *Black bars*, WT; *white bars*, *Scn1b* null ($n = 24$ cells/genotype). Significant differences from WT are indicated as follows: *, $p < 0.05$; **, $p < 0.01$; ***, $p < 0.001$. *Error bars*, S.E.

detail, the maximum rates of depolarization and repolarization were calculated from the differentiated waveform of the AP (Fig. 7*C*). The first derivative of V_m showed a single depolarizing peak (I_{Na}) and two repolarizing peaks, similar to previous results (27, 28). Consistent with our immunohistochemistry results showing no changes in cell surface expression of $Na_v1.8$, we observed no significant changes in the rate of the AP upstroke in the absence of *Scn1b* ($p = 0.111$; Fig. 7*D*). In contrast, the rate of the first component of the repolarizing phase was increased in *Scn1b* null small DRG neurons compared with WT ($p = 0.0001$; Fig. 7*D*).

To determine how the observed increased rate of repolarization would affect the excitability of *Scn1b* null neurons, we applied a 1000-ms depolarizing pulse of 1.5 times the threshold current to examine neuronal firing. We observed that eight of nine WT cells fired a single AP in response to this stimulus. A typical WT result is shown in Fig. 8*A* (*black trace*). In contrast, seven of nine *Scn1b* null neurons fired a train of more than 20 APs in response to the stimulus (Fig. 8*B*, *bottom*). A typical *Scn1b* null recording is shown in Fig. 8*A* (*gray trace*). These results are quantified in Fig. 8*B*. We calculated a mean of 1.3 ± 0.3 APs/cell for WT *versus* 23.3 ± 5.5 APs/cell for *Scn1b* null (Fig. 8*B*, *top*; $p = 0.00099$). We next applied a train of 12 pulses to 1.5× threshold current, 3 ms long, paced at 10 Hz. Under these conditions, both genotypes generated APs with similar properties (Fig. 8*C*). Results of analysis of the differentiated AP waveforms generated at this frequency showed that the initial upstroke rate was increased slightly in null neurons compared with WT (Fig. 8*D*, *top*, *1st AP*; $p = 0.054$). Repeating the same pulse every 100 ms, we observed that the upstroke rate of the twelfth AP was significantly increased for *Scn1b* null neurons compared with WT (Fig. 8*D*, *top*, *12th PA*; $p = 0.009$), reflecting less accumulation of I_{Na} inactivation in null neurons compared with WT. In addition, the rate of repolarization was increased for null neurons compared with WT for the first threshold pulse as well as for the twelfth pulse (Fig. 8*D*, *bottom*; $p = 0.009$ and $p = 0.008$, respectively).

Effect of Scn1b deletion on I_{to} Density—I_{to} serves to repolarize the neuronal membrane following depolarizing events and to stabilize the membrane potential below the firing threshold (29). Thus, differential regulation of this current is expected to modify neuronal excitability. Because K^+ channels responsible for I_{to} in heart have been shown to be modified by *Scn1b in vitro* (30, 31), we asked whether I_{to} may be modulated by *Scn1b* deletion in DRGs *in vivo* and thus contribute to hyperexcitability. I_{to} was recorded as described under "Experimental Procedures." We observed a 40–50% reduction in I_{to} density in *Scn1b* null compared with WT neurons (Fig. 8*E*, $n = 7$ WT and $n = 10$ null). We postulate

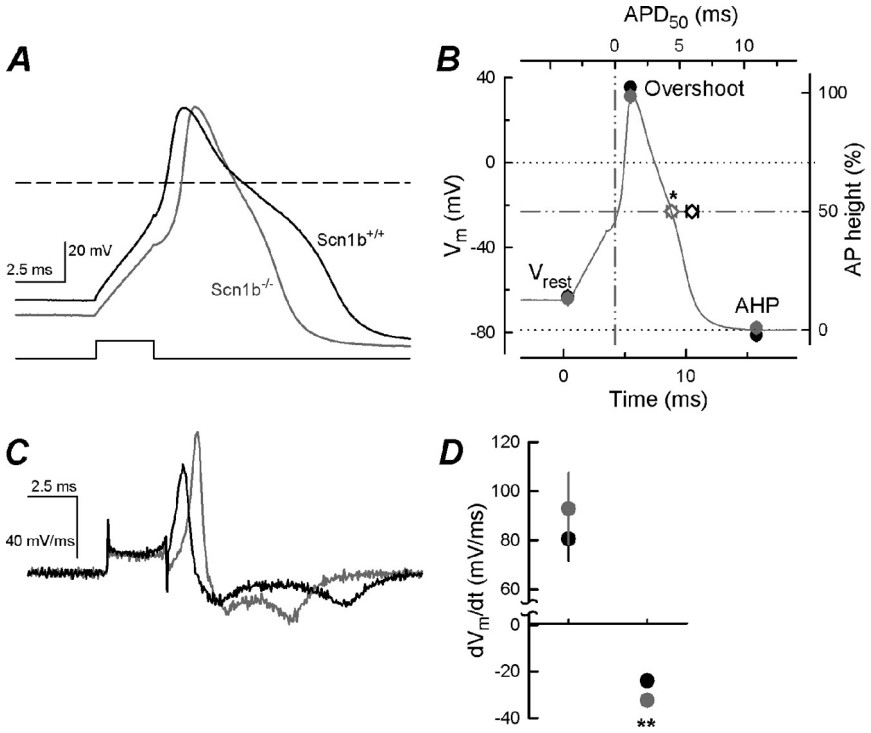

FIGURE 7. ***Scn1b* null neurons have altered AP kinetics.** *A*, representative APs were recorded from one WT (*black*) and one *Scn1b* null (*gray*) neuron. APs were evoked by a 3-ms current pulse (*lower trace*) to threshold. *B*, AP parameters, including V_{rest}, overshoot, and AHP, expressed in mV, for WT ($n = 11$; *black symbols*) or *Scn1b* null ($n = 12$; *gray symbols*) small DRG neurons. AP duration at half of the maximal spike amplitude (ADP_{50}; *diamonds*) is indicated in the *top x axis*. The AP trace shown is taken from *A* (*Scn1b* null). *C*, corresponding dV_m/dt of the APs shown in *A*. *D*, maximum upstroke rate and maximum rate of the first repolarization phase (first negative peak in *C*). *Symbols* and *cells* are as in *B*. **, significant difference from WT at $p < 0.01$. *Error bars*, S.E.

that this reduction in I_{to} may underlie the observed hyperexcitability of *Scn1b* null DRG neurons.

DISCUSSION

The overall conclusion of this work is that *Scn1b* null nociceptive neurons are hyperexcitable, suggesting that *Scn1b* plays an important role in maintaining normal excitability and, with that pain sensation, in WT DRGs. *Scn1b* deletion results in complex effects on I_{Na} and I_K expression which, taken together, tip the balance toward increased excitability in DRG neurons *in vivo*. A depolarizing shift in the voltage dependence of VGSC inactivation (resulting in greater channel availability), decreased persistent I_{Na}, decreased $\tau_{deact,fast}$, and a decreased proportion of slow inactivated I_{Na} are all consistent with changes in the AP favoring hyperexcitability, including the observed shortened APD_{50} and increased rate of AP repolarization. Decreased levels of $Na_v1.9$ at the plasma membrane in response to *Scn1b* deletion are also consistent with hyperexcitability because this change is predicted to result in reduced levels of slowly inactivating or non-inactivating I_{Na}. Finally, the observation of decreased levels of I_{to} in DRG neurons in our model is consistent with previous reports in other sensory neuron models, including suppression of A-type (transient outward) I_K, leading to enhanced excitability of pancreas-specific afferent neurons in chronic pancreatitis (32), and reduced A-type I_K in gastric sensory ganglion neurons, leading to hyperexcitability in a model of inflammation and gastric ulcers (33). Interestingly, our observation of slowed VGSC recovery from inactivation in *Scn1b* null DRG neurons would suggest hypoexcitability if examined in isolation. However, this effect is outweighed by other changes *in vivo* because overall the sum of the observed effects of *Scn1b* deletion result in DRG neuron hyperexcitability. We conclude that the role of *Scn1b* in DRG neurons *in vivo* is to dampen excitability by predominantly shifting the voltage dependence of I_{Na} inactivation in the hyperpolarizing direction and increasing the level of persistent I_{Na}. In addition, through a mechanism that is not yet understood, *Scn1b* increases I_{to}.

Although the severe and ultimately lethal phenotype of *Scn1b* null mice (13) precludes a behavioral study of pain, our results predict that these mice have allodynia. Importantly, our data may be translated to imply that human patients with inherited *SCN1B*-mediated $GEFS^+$ epilepsies (34), especially patients with two inherited functional null *SCN1B* mutant alleles resulting in Dravet syndrome (35), may have increased sensitivity to pain.

Scn1b null mice display a hyperexcitable CNS phenotype (13). Using a combination of heterologous cells and native CNS neurons, we reported previously that *Scn1b* effectively imposes a "break" on excitability in brain, stabilizing VGSC closed states at hyperpolarized potentials and inactivated states at depolarized potentials (36). The present study further supports the idea that *Scn1b* exerts critical controls to limit neuronal excitability and extends this knowledge to the peripheral nervous system.

A growing body of evidence suggests that *Scn1b* and the K^+ channel subunits underlying I_{to} are structurally and functionally associated. In a heterologous system, $\beta 1$

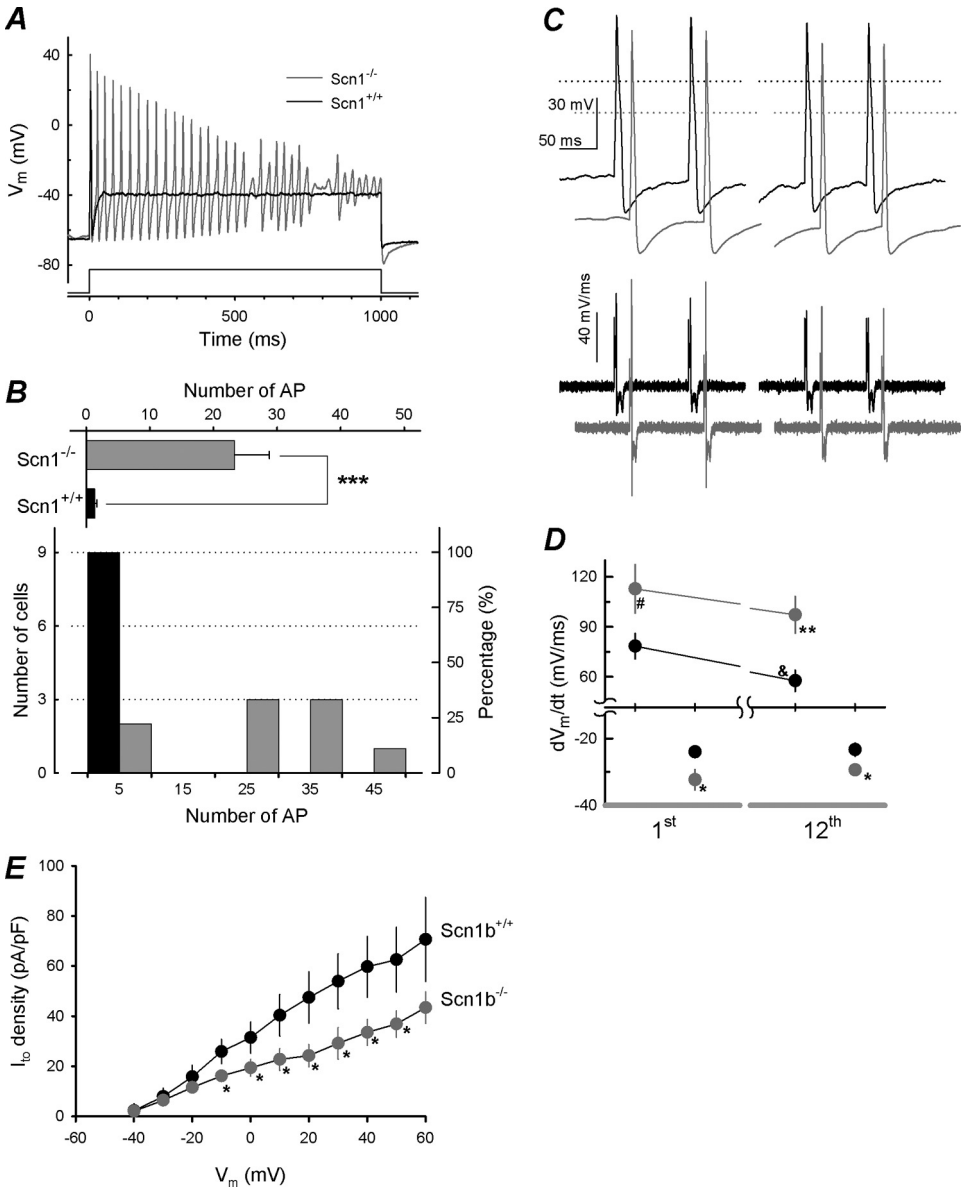

FIGURE 8. ***Scn1b* null neurons are hyperexcitable.** *A*, typical recordings from WT (*black*) or *Scn1b* null (*gray*) small DRG neurons in response to a depolarizing current pulse (1.5× threshold current) with a duration of 1000 ms (*bottom trace*). *B*, *bottom*, histogram of the number of APs fired for each WT (*black bars*) or *Scn1b* null (*gray bars*) cell recorded in response to the depolarizing pulse described in *A*; *numbers* represent the center of each bin, and each bin is 10 APs wide. *Top*, average of firing, ($n = 9$ neurons/group). *C*, AP recordings in response to a train of depolarizing pulses (12 pulses, 10 Hz, 1.5× threshold current). The first two and last two APs are shown for a cell of each genotype (*top panel*) with the corresponding dV_m/dt traces (*bottom*). The base line has been displaced for presentation proposes only. *D*, maximum upstroke rate and the maximum rate of the repolarization phase measured from the first and twelfth AP recordings using the 10-Hz train protocol for WT ($n = 7$; *black circles*) or *Scn1b* null ($n = 8$; *gray circles*) small DRG neurons. *E*, I_{to} density for WT ($n = 7$; *black circles*) or *Scn1b* null ($n = 10$; *gray circles*) small DRG neurons. Significant difference from WT is shown as follows: #, $p < 0.06$; *, $p < 0.05$; **, $p < 0.01$; ***, $p < 0.001$. Significant difference from the first AP is shown as follows: &, $p < 0.06$.

increases I_K density and modulates I_K gating generated by $K_v4.3$ expression (31). In neonatal rat ventricular myocytes, *Scn1b* silencing results in reduction of KChIP2 mRNA and protein as well as $K_v4.x$ proteins, with the outcome of decreased I_{to} in addition to decreased I_{Na} (30). Our observation of decreased I_{to} in *Scn1b* null DRGs supports these previous studies and extends those results to include peripheral neurons. Taken together, these data suggest that I_{Na} and I_K may be structurally associated through VGSC $\beta1$ subunits and, further, that *Scn1b* plays a critical role in regulating AP properties in addition to modulation of I_{Na}, thus exerting sensitive and multifaceted control over neuronal excitability. Because of this, we propose that $\beta1$ and/or $\beta1B$, encoded by *SCN1B*, may be novel targets for development of pain therapeutics.

REFERENCES

1. Brackenbury, W. J., Djamgoz, M. B., and Isom, L. L. (2008) *Neuroscientist* **14,** 571–583
2. Brackenbury, W. J., and Isom, L. L. (2008) *Expert Opin. Ther. Targets* **12,** 1191–1203
3. Patino, G. A., and Isom, L. L. (2010) *Neurosci. Lett.* **486,** 53–59
4. Lopez-Santiago, L. F., Pertin, M., Morisod, X., Chen, C., Hong, S., Wiley, J., Decosterd, I., and Isom, L. L. (2006) *J. Neurosci.* **26,** 7984–7994
5. Kazen-Gillespie, K. A., Ragsdale, D. S., D'Andrea, M. R., Mattei, L. N.,

Rogers, K. E., and Isom, L. L. (2000) *J. Biol. Chem.* **275,** 1079–1088
6. Blackburn-Munro, G., and Fleetwood-Walker, S. M. (1999) *Neuroscience* **90,** 153–164
7. Klugbauer, N., Lacinova, L., Flockerzi, V., and Hofmann, F. (1995) *EMBO J.* **14,** 1084–1090
8. Sangameswaran, L., Fish, L. M., Koch, B. D., Rabert, D. K., Delgado, S. G., Ilnicka, M., Jakeman, L. B., Novakovic, S., Wong, K., Sze, P., Tzoumaka, E., Stewart, G. R., Herman, R. C., Chan, H., Eglen, R. M., and Hunter, J. C. (1997) *J. Biol. Chem.* **272,** 14805–14809
9. Vijayaragavan, K., O'Leary, M. E., and Chahine, M. (2001) *J. Neurosci.* **21,** 7909–7918
10. Sangameswaran, L., Delgado, S. G., Fish, L. M., Koch, B. D., Jakeman, L. B., Stewart, G. R., Sze, P., Hunter, J. C., Eglen, R. M., and Herman, R. C. (1996) *J. Biol. Chem.* **271,** 5953–5956
11. Vijayaragavan, K., Powell, A. J., Kinghorn, I. J., and Chahine, M. (2004) *Biochem. Biophys. Res. Commun.* **319,** 531–540
12. Dib-Hajj, S., Black, J. A., Cummins, T. R., and Waxman, S. G. (2002) *Trends Neurosci.* **25,** 253–259
13. Chen, C., Westenbroek, R. E., Xu, X., Edwards, C. A., Sorenson, D. R., Chen, Y., McEwen, D. P., O'Malley, H. A., Bharucha, V., Meadows, L. S., Knudsen, G. A., Vilaythong, A., Noebels, J. L., Saunders, T. L., Scheuer, T., Shrager, P., Catterall, W. A., and Isom, L. L. (2004) *J. Neurosci.* **24,** 4030–4042
14. Lopez-Santiago, L. F., Meadows, L. S., Ernst, S. J., Chen, C., Malhotra, J. D., McEwen, D. P., Speelman, A., Noebels, J. L., Maier, S. K., Lopatin, A. N., and Isom, L. L. (2007) *J. Mol. Cell Cardiol.* **43,** 636–647
15. Brackenbury, W. J., and Djamgoz, M. B. (2006) *J. Physiol.* **573,** 343–356
16. Okuse, K., Malik-Hall, M., Baker, M. D., Poon, W. Y., Kong, H., Chao, M. V., and Wood, J. N. (2002) *Nature* **417,** 653–656
17. Shah, B. S., Rush, A. M., Liu, S., Tyrrell, L., Black, J. A., Dib-Hajj, S. D., and Waxman, S. G. (2004) *J. Neurosci.* **24,** 7387–7399
18. Abdulla, F. A., and Smith, P. A. (2002) *J. Neurophysiol.* **88,** 2518–2529
19. Abdulla, F. A., and Smith, P. A. (2001) *J. Neurophysiol.* **85,** 644–658
20. Cummins, T. R., and Waxman, S. G. (1997) *J. Neurosci.* **17,** 3503–3514
21. Rush, A. M., Bräu, M. E., Elliott, A. A., and Elliott, J. R. (1998) *J. Physiol.* **511,** 771–789
22. Wood, J. N., Boorman, J. P., Okuse, K., and Baker, M. D. (2004) *J. Neurobiol.* **61,** 55–71
23. Akopian, A. N., Souslova, V., England, S., Okuse, K., Ogata, N., Ure, J., Smith, A., Kerr, B. J., McMahon, S. B., Boyce, S., Hill, R., Stanfa, L. C., Dickenson, A. H., and Wood, J. N. (1999) *Nature* **402,** 541–548
24. Priest, B. T., Murphy, B. A., Lindia, J. A., Diaz, C., Abbadie, C., Ritter, A. M., Liberator, P., Iyer, L. M., Kash, S. F., Kohler, M. G., Kaczorowski, G. J., MacIntyre, D. E., and Martin, W. J. (2005) *Proc. Natl. Acad. Sci. U.S.A.* **102,** 9382–9387
25. Goldstein, M. E., House, S. B., and Gainer, H. (1991) *J. Neurosci. Res.* **30,** 92–104
26. Decosterd, I., Ji, R. R., Abdi, S., Tate, S., and Woolf, C. J. (2002) *Pain* **96,** 269–277
27. Blair, N. T., and Bean, B. P. (2002) *J. Neurosci.* **22,** 10277–10290
28. Bean, B. P., (2007) *Nat. Rev. Neurosci.* **8,** 451–465
29. Safronov, B. V., Bischoff, U., and Vogel, W. (1996) *J. Physiol.* **493,** 393–408
30. Deschênes, I., Armoundas, A. A., Jones, S. P., and Tomaselli, G. F. (2008) *J. Mol. Cell Cardiol.* **45,** 336–346
31. Deschênes, I., and Tomaselli, G. F. (2002) *FEBS Lett.* **528,** 183–188
32. Xu, G. Y., Winston, J. H., Shenoy, M., Yin, H., and Pasricha, P. J. (2006) *Am. J. Physiol. Gastrointest. Liver Physiol.* **291,** G424–G431
33. Dang, K., Bielefeldt, K., and Gebhart, G. F. (2004) *Am. J. Physiol. Gastrointest. Liver Physiol.* **286,** G573–G579
34. Scheffer, I. E., Harkin, L. A., Grinton, B. E., Dibbens, L. M., Turner, S. J., Zielinski, M. A., Xu, R., Jackson, G., Adams, J., Connellan, M., Petrou, S., Wellard, R. M., Briellmann, R. S., Wallace, R. H., Mulley, J. C., and Berkovic, S. F. (2007) *Brain* **130,** 100–109
35. Patino, G. A., Claes, L. R., Lopez-Santiago, L. F., Slat, E. A., Dondeti, R. S., Chen, C., O'Malley, H. A., Gray, C. B., Miyazaki, H., Nukina, N., Oyama, F., De Jonghe, P., and Isom, L. L. (2009) *J. Neurosci.* **29,** 10764–10778
36. Aman, T. K., Grieco-Calub, T. M., Chen, C., Rusconi, R., Slat, E. A., Isom, L. L., and Raman, I. M. (2009) *J. Neurosci.* **29,** 2027–2042